Novel OCDM Transceiver Design for Doubly-Dispersive Channels

Hamza Haif, *Graduate Student Member, IEEE*, Salah Eddine Zegrar, *Graduate Student Member, IEEE*, and Hüseyin Arslan, *Fellow, IEEE*

***Abstract*—Orthogonal chirp division multiplexing (OCDM) is a new multi-carrier scheme that has been emerging as a new candidate for 6G waveform taking advantage of the unique features of the chirp spread spectrum that makes it immune to intersymbol interference raised due to delay spread. However, a thorough analysis of OCDM under doubly-dispersive channels has not been conducted yet to verify its robustness against Doppler spread as well. In this paper, we investigate the input-output relationship of an OCDM system under doubly-selective channel, where we demonstrate that the circular convolution property of OCDM partially holds even under Doppler spread. Building on previous results, we show the difficulties and problems associated with estimating and equalizing the channel at the receiver side in conventional OCDM systems, especially in case of having fractional delay and Doppler shifts. Then, we propose a new OCDM transceiver by adding fast Fourier transform (FFT) and windowing blocks to ensure channel tap separability and reduce the effect of fractional Doppler shift, respectively. Accordingly, a new channel estimation scheme is developed for the proposed OCDM system. The numerical and simulation results validate the advantages of the proposed OCDM system performance under doubly-dispersive channels over the conventional where the proposed leverages a bit-error-rate (BER) gain in perfect channel state information (CSI) of 2 dB and 3 dB for minimum mean squared error (MMSE) and message passing (MP) equalizers, respectively, and show that it holds great promise as an emerging radio access technology for 6G wireless systems.**

***Index Terms*—Channel estimation, discrete Fresnel transform, doubly-dispersive channels, OCDM.**

I. Introduction

THE continuation of various facets of our lives including education, trading, banking, healthcare, transportation, etc., over the last couple of years has largely been due to the reliable connectivity provided via cellular and WiFi networks. A major reason for this is the paradigm shift promised by the 5th generation (5G) of wireless communication, where the focus moved from merely high data rates to strict reliability, low latency, and massive connectivity [1]. Furthermore, the proliferation of Internet of Things (IoT) devices, in conjunction with various emerging applications, presents a significant hurdle in the development of a new physical (PHY) layer that guarantees dependable and equitable communication for these aforementioned applications [2].

However, unlike previous generations, 5G did not introduce a completely new PHY layer design. Rather the concept of numerology, i.e., different sets of values for PHY parameters such as subcarrier spacing and cyclic prefix (CP) duration was proposed [3]. This was partially to ensure backward compatibility, and partially because none of the other proposed designs outperformed orthogonal frequency division multiplexing (OFDM) in all aspects. Given that 6th generation (6G) will stretch the communication fabric further to include different frequency bands, (beyond communication) applications, environments, and network architectures/deployments, it is necessary to look at other waveforms that can fulfill these requirements and applications along with OFDM [4].

A new vision for 6G waveforms is that the waveform design should be done in a manner where the data symbols are spread across both domains of dispersiveness (time and frequency) in order to make all the data symbols go through the same channel gain [5]. In this light, several waveforms have been proposed to provide better performance compared to OFDM. Orthogonal Time-Frequency Space (OTFS) a 2D modulation scheme that spreads data in the delay-Doppler domain that is shown to have a superior performance in highly mobile scenarios [6], OTFS is able to construct a sparse delay-Doppler channel impulse response to enable efficient high Doppler channel estimation [7]. Motivated by OTFS a multicarrier orthogonal delay-Doppler division multiplexing (ODDM) modulation is proposed to couple the modulated signal with the delay-Doppler representation of a doubly-selective channel [8]. Using a chirp based frequency varying basis as a multicarrier transmission scheme, the authors in [9] introduced an Affine Frequency Division Multiplexing (AFDM) waveform based on Affine Fourier Transform (AFT) rather than conventional Fourier Transform, multiplexing the data in the discrete-AFT domain allows the separability of channel paths along with obeying equal gain criteria by making the data symbols experience the same path coefficients.

Recently, orthogonal chirp division multiplexing (OCDM) has garnered attention as a promising new waveform for high-data-rate communication. It is a modulation technique that spreads the data over time and the entire signal bandwidth by modulating them using orthogonal chirps based on the discrete

Manuscript received 31 May 2023; revised 5 December 2023 and 4 January 2024; accepted 21 February 2024. Date of publication 29 February 2024; date of current version 15 August 2024. This work was supported by the Scientific and Technological Research Council of Turkey (TUBITAK) under Grant 123E514. The review of this article was coordinated by Dr. Xiaohu Ge. *(Corresponding author: Hamza Haif.)*

The authors are with the Department of Electrical and Electronics Engineering, Istanbul Medipol University, Istanbul 34810, Türkiye (e-mail: hamza.haif@std.medipol.edu.tr; salah.zegrar@std.medipol.edu.tr; huseyinarslan@medipol.edu.tr).

Digital Object Identifier 10.1109/TVT.2024.3371708

Fresnel transform (DFnT), which makes it more robust against multi-path propagation and frequency-selective channels [10]. Moreover, OCDM can be a potential candidate waveform for 5G and beyond wireless communication for several reasons [11]. First, the chirp spread-spectrum-based system is widely used in radar applications for its inherent robustness to Doppler shifts, which makes it suitable for joint sensing and communication applications as done in the work of [10]. Second, OCDM systems are compatible with OFDM modulation since DFnT is related to discrete Fourier transform (DFT) which is a condition for backward compatibility.

Even though OCDM sounds attractive based on the aforementioned features, further elaboration and studying were needed for the OCDM waveform. A thorough analysis of OCDM impairments in [11] revealed that OCDM is more resilient to narrowband interference, and coded OCDM performance is better than coded OFDM under frequency selective channels. In addition, analyzing the spectrum of OCDM in [12] showed that it is difficult to mitigate out-of-band emission (OOBE) by introducing guard bands due to the chirp property that spans the whole bandwidth, so the authors introduce a digitally filtered OCDM to further shape the spectrum. Moreover, the inseparability of the data symbols in both time and frequency domains makes channel estimation in wireless communication quite challenging. By using the Zadoff-Chu sequences as pilots, the authors in [13] proposed a minimum mean squared error (MMSE) model to estimate the frequency selective channel in the time domain for OCDM. In [14], different frequency-domain pilot multiplexing OCDM schemes are investigated under frequency selective channels. Channel estimation for OCDM with carrier frequency offset (CFO) is proposed in [15], where a CP is added to the transmitted signal and used for CFO effect compensation while sub-chirp pilots are superimposed for channel, estimation purposes. In [16], the performance of OCDM under time-varying underwater acoustic channels was studied, and the channel estimation algorithm is proposed by exploiting the circular convolution characteristics of DFnT. The effects of time and frequency shifts individually or jointly in the Fresnel domain are analyzed in [17]. The authors provided a closed-form expression for the discrete-Fresnel domain radar channel estimation, and the study was extended to consider multiple-input multiple-output (MIMO), and joint radar and communication (JRC) operation. In [18] a multi-carrier wideband OCDM waveform is used to exploit the coherence bandwidth of thr THz channel for automotive radar applications.

However, most of the research conducted on OCDM considers only static channels [13], [14], [15], [16], or static channels with single frequency offset [17], [18]. As the 6G systems are expected to support a high throughput rate at even higher mobility when compared to 5G systems, there is a need to investigate the behavior of OCDM under doubly-dispersive channels. Moreover, we will show that under doubly-dispersive channel, fractional Doppler shifts causes spreading in both delay and Doppler domains.

This paper presents an analysis and investigation of the OCDM waveform for next-generation networks, utilizing a novel approach to examine the waveform. In this study, we investigate the input-output correlation within the chirp domain under the influence of doubly-dispersive channels. Our findings reveal that the time domain channel delays and the Doppler shifts are jointly combined within the chirp domain. We present also a novel OCDM transceiver design that offers the capability of channel taps separability through the incorporation of additional fast Fourier transform (FFT) blocks. Furthermore, we address the issue of fractional Doppler by implementing a windowing receiver to mitigate its effects. The contributions of this work are summarized as follows:

- While most OCDM studies focus on static channels or channels with a single frequency shift, we are the first to present a full analysis of the input-output relationship of the OCDM waveform in the chirp domain, considering the impact of a doubly dispersive channel. The input-output relationship indicates that the effective channel in the chirp domain results in shifts of the received signal by delays equivalent to the summation of the time domain delay and Doppler shifts of each tap. Based on that, we generalize the circular convolution property of OCDM for the doubly-selective channels.
- We demonstrate that doubly-dispersive channels in time-frequency are selective-dispersive in chirp domain, where depending on the delay and Doppler shift values the channel taps the effective channel can be selective, dispersive, or selective and dispersive simultaneously.
- We propose a novel OCDM system design that leverages an additional FFT block at the receiver and transmitter to provide an effective sparse channel with separable taps. The introduced FFT blocks can provide channel resolvability by separating the combination of delay and Doppler shifts in the chirp domain.
- As a solution for fractional Doppler that causes spreading in the chirp domain (inter-chirp interference), the proposed system incorporates a Kaizer window block to effectively mitigate the sidelobe tails of the received signal that are induced by fractional Doppler shifts.
- We proposed a novel channel estimation for the designed OCDM frame, where two embedded symbols in the chirp domain are exploited as pilots. These pilots are surrounded by a guard to avoid interference between pilots and data symbols.
- The performance of the proposed OCDM system is verified using bit error rate (BER) performance where the performance of the channel estimation technique is proven to leverage an NMSE gain of 5 dB in the presence of fractional Doppler shifts using windowing techniques. Both performances emphasize the superiority of the proposed schemes. Then, message passing (MP) detector is developed to mitigate the impact of the channel, effectively leveraging channel diversity to improve the overall performance of the system.

The paper is organized as follows; In Section II, the input-output relationship of the OCDM waveform in chirp domain is derived. Then, a novel OCDM framework is proposed in Section III. In Section IV, a channel estimation technique based on windowing and embedded pilots is introduced. Section V

provides a performance analysis for the proposed framework. Finally concluding points are provided in Section VI. [1]

II. OCDM Input-Output Relationship

A. OCDM Transmitted Signal

In this work, we consider an OCDM transmission spanning a bandwidth B and time duration T, where a set of N orthogonal chirps are used to modulate N data symbols $\mathbf{x}$ using the inverse discrete Fresnel transform (IDFnT). The discrete time-domain baseband OCDM signal is given as [10]

$$s(m) = e^{j\frac{\pi}{4}} \frac{1}{\sqrt{N}} \sum_{n=0}^{N-1} x(n) e^{-j\frac{\pi}{N}(m-n)^2} \tag{1}$$

To cast (1) from serial to matrix-vector form, we define $\mathbf{\Phi}$ to be the $\mathbb{C}^{N\times N}$ unitary DFnT matrix; then, (1) is rewritten as

$$\mathbf{s} = \mathbf{\Phi}^H \mathbf{x}, \tag{2}$$

where, the $(m,n)^{th}$ element in $\mathbf{\Phi}$ is given by

$$\Phi(m,n) = \frac{1}{\sqrt{N}} e^{-j\frac{\pi}{4}} e^{j\frac{\pi}{N}(m-n)^2}, \quad [N]_2 = 0. \tag{3}$$

As seen from (3), $\mathbf{\Phi}$ can be decomposed to a DFT matrix with additional quadratic phases using the following relation

$$\mathbf{\Phi} = \mathbf{\Theta}_1 \mathbf{F} \mathbf{\Theta}_2, \tag{4}$$

where, the additional quadratic phases are diagonal matrices given by $\Theta_1(m,m) = e^{-j\frac{\pi}{4}} e^{j\frac{\pi}{N}m^2}$ and $\Theta_2(m,m) = e^{j\frac{\pi}{N}n^2}$ with $[N]_2 = 0$. $\mathbf{F}$ denotes the unitary DFT matrix.

B. OCDM Received Signal Model

Let $h(\tau,\nu)$ be a doubly-dispersive channel with the following delay-Doppler impulse response

$$h(\tau,\nu) = \sum_{i=0}^{L-1} h_i \delta\left(\tau - \frac{l_i}{B}\right) \delta\left(\nu - \frac{k_i}{T}\right), \tag{5}$$

where L, h_i, l_i, and k_i denote the number of propagation paths, the channel gain, the integer delay, and Doppler shift of the i-th reflector, respectively.

After the transmitted signal passes through the wireless propagation channel, the received signal is found as

$$\mathbf{r} = \mathbf{H}\mathbf{\Phi}^H \mathbf{x} + \mathbf{w}, \tag{6}$$

where $\mathbf{H}$ and $\mathbf{w}$ represent the time channel matrix and the additive white Gaussian noise (AWGN) vector with variance σ^2, respectively. Specifically, $\mathbf{H}$ is given as

$$\mathbf{H} = \sum_{i=0}^{L-1} h_i \mathbf{\Pi}_N^{l_i} \mathbf{\Delta}_N^{k_i}, \tag{7}$$

where $\mathbf{\Pi}_N^{l_i}$ is the $N\times N$ permutation matrix with $\Pi_N^{l_i}(l,k) = \delta([l-k]_N - l_i)$, and $\mathbf{\Delta}_N$ represents the $N\times N$ diagonal matrix

$$\mathbf{\Delta}_a^{k_i} = \text{diag}\left[z_i^0, z_i^1, \ldots, z_i^{(a-1)}\right], \tag{8}$$

with $z_i = e^{\frac{j2\pi k_i}{N}}$. So (7) is reformulated to

$$\begin{aligned} H(l,k) &= \sum_{k'=0}^{N-1}\sum_{i=0}^{L-1} h_i \delta([l-k']_N - l_i) e^{j2\pi\frac{k_i k'}{N}} \delta(k-k'), \\ &= \sum_{i=0}^{L-1} h_i \delta([l-k]_N - l_i) e^{j2\pi\frac{k_i k}{N}}. \end{aligned} \tag{9}$$

At the receiver side, the received signal is converted to chirp domain by applying DFnT as follow

$$\mathbf{y} = \mathbf{\Phi}\mathbf{r} = \mathbf{H}_{\text{eff}}\mathbf{x} + \mathbf{\Phi}\mathbf{w}, \tag{10}$$

where $\mathbf{H}_{\text{eff}} = \mathbf{\Phi}\mathbf{H}\mathbf{\Phi}^H$ denotes the chirp-domain effective channel matrix. Since $\mathbf{\Phi}$ is a unitary matrix, $\mathbf{\Phi}\mathbf{w}$ is an AWGN with the same statistical properties of $\mathbf{w}$; in the rest of the paper, we are going to use only $\mathbf{w}$ as notation for the AWGN.

$\mathbf{H}_{\text{eff}}$ can be computed using (3) and (9) as follows

$$\begin{aligned} H_{\text{eff}}(m,n) &= \sum_{l=0}^{N-1}\sum_{k=0}^{N-1}\sum_{i=0}^{L-1} \Phi(m,l) H(l,k) \Phi^H(k,n), \\ &= \sum_{i=0}^{L-1} h_i e^{j\pi\frac{(m^2-n^2)}{N}} \sum_{l=0}^{N-1}\sum_{k=0}^{N-1} e^{j\pi\frac{(l^2-2ml-k^2+2kn+2kk_i)}{N}} \\ &\quad \times \delta([l-k]_N - l_i). \end{aligned} \tag{11}$$

Simplifying (11), we find

$$\begin{aligned} H_{\text{eff}}(m,n) = \sum_{l=0}^{N-1}\sum_{i=0}^{L-1} h_i e^{j\pi\frac{(m^2-n^2)}{N}} e^{-j\frac{2\pi}{N}(\frac{l_i^2}{2}+l_i n+k_i l_i)} \\ \times e^{-j\frac{2\pi}{N}l(m-n+l_i+k_i)}. \end{aligned} \tag{12}$$

Let $A_{\text{i}}(m,n) = \sum_{l=0}^{N-1} e^{-j\frac{2\pi}{N}l(m-n+l_i+k_i)}$, where A_{i} is non zero only if $[n-m]_N = l_i + k_i$, i.e.,

$$A_{\text{i}}(m,n) = \begin{cases} 1, & [n-m]_N = (l_i+k_i) \\ 0, & \text{Otherwise.} \end{cases} \tag{13}$$

By substituting (12) in (10), the input-output relationship can be expressed as

$$\begin{aligned} y(m) &= \sum_{n=0}^{N-1} H_{\text{eff}}(m,n) x(n) \\ &= \sum_{n=0}^{N-1} x(n) \sum_{i=0}^{L-1} h_i e^{j\pi\frac{(m^2-n^2)}{N}} e^{-j\frac{2\pi}{N}(\frac{l_i^2}{2}+l_i n+k_i l_i)} \\ &\quad \times \delta([n-m]_N - (l_i+k_i)) + w(m). \end{aligned} \tag{14}$$

[1] *Notation:* Bold uppercase $\mathbf{A}$, bold lowercase $\mathbf{a}$, and unbold letters A, a denote matrices, column vectors, and scalar values, respectively. $(\cdot)^H$, $(\cdot)^T$, and $(\cdot)^{-1}$ denote the Hermitian, transpose, and inverse operators. $[\alpha]_\beta$ takes modulo-β of α. $\delta(\cdot)$ denotes the Dirac-delta function. $\text{diag}(A_1,\ldots,A_N)$ returns the diagonal and matrix composed of $A_1,\ldots,A_N$ in its diagonal. $\mathbb{C}^{M\times N}$ denotes the space of $M\times N$ complex-valued matrices. Symbol j represents the imaginary unit of complex numbers with $j^2 = -1$.

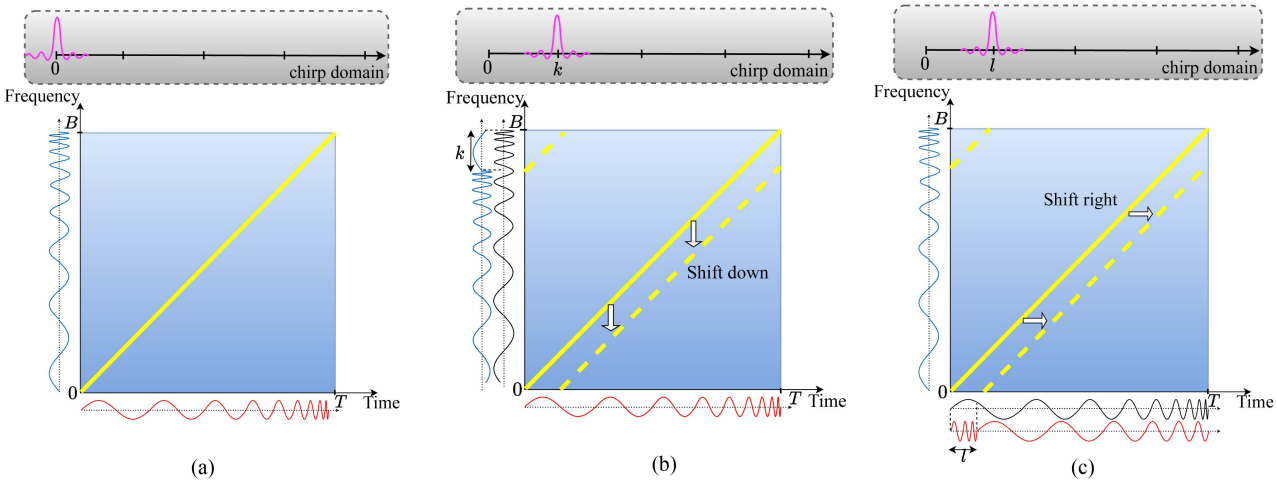

Fig. 1. Spectrogram of the an OCDM carrier under time and frequency dispersions. (a) No dispersion. (b) Dispersion with k shift in frequency. (c) Dispersion with l shift in time.

Therefore,

$$y(m) = \sum_{i=0}^{L-1} h_i e^{j\frac{\pi}{N}\left(m^2-([m-l_i-k_i]_N)^2\right)} \times e^{-j\frac{2\pi}{N}\left(\frac{l_i^2}{2}+l_i[m-l_i-k_i]_N+k_i l_i\right)} \times x\left([m-l_i-k_i]_N\right) + w(m). \tag{15}$$

By simplifying (15), we find

$$y(m) = \sum_{i=0}^{L-1} \hbar_i e^{j\frac{2\pi}{N}k_i(m-[l_i+k_i])} x\left([m-l_i-k_i]_N\right) + w(m), \tag{16}$$

where $\hbar_i = h_i e^{j\pi\frac{k_i^2}{N}}$. Note that the result given by (16) shows that the received signal can be seen as the result of transmitting $\mathbf{x}$ over a doubly-dispersive channel with $\hat{h}_i, l_i + k_i$, and k_i channel gain, delay, and Doppler shift respectively.

Lemma: Let $\mathbf{H}\{h, l, k\}$ be the time-domain doubly dispersive channel matrix which is as a function of channel gains $h = [h_0, \ldots, h_{L-1}]$, delays $l = [l_0, \ldots, l_{L-1}]$, and Doppler shifts $k = [k_0, \ldots, k_{L-1}]$. Transmitting a time-domain OCDM signal ($\mathbf{x}_{\text{time}} = \mathbf{\Phi}\mathbf{x}_{\text{chirp}}$) through a doubly-dispersive channel with h channel gains, l delays, and k Doppler shifts results in a chirp-domain OCDM signal ($\mathbf{x}_{\text{chirp}}$) passing through a doubly-dispersive channel with $he^{j\pi\frac{k^2}{N}}$ channel gains, $l + k$ delays, and k Doppler shifts, i.e.,

$$\mathbf{H}\{h, l, k\}\mathbf{x}_{\text{time}} \equiv \mathbf{H}\{he^{j\pi\frac{k^2}{N}}, l + k, k\}\mathbf{x}_{\text{chirp}}. \tag{17}$$

Fig. 1(a) depicts the spectrogram of a chirp that is spread in both time and frequency domains. The aforementioned spread becomes localization in the chirp domain wherein a single chirp becomes an impulse in the chirp domain. The impact of delays and Doppler shifts on the OCDM waveform as stated in (16) is shown in Fig. 1(b) and (c), respectively. It is observed that both time and Doppler shifts result in a shift in the chirp domain. Specifically, if the frequency shift is equal to the time delay i.e., $l = k$, as illustrated in Fig. 1(b) and (c), the same shift occurs in the chirp domain. Consequently, in OCDM systems, it is difficult to distinguish between the source of the shift if it is due to time or frequency shifts.

Special case: in case of the static channel (i.e., $k = 0$), (17) becomes the conventional DFnT circular convolution property which states that the DFnT of the convolution of two circular matrices results in a convolution of one matrix with DFnT of the other matrix [15], [16], as follow

$$\mathbf{H}\{h, l, 0\}\mathbf{x}_{\text{time}} \equiv \mathbf{H}\{he^{j\pi\frac{0^2}{N}}, l + 0, 0\}\mathbf{x}_{\text{chirp}}, \equiv \mathbf{H}\{h, l, 0\}\mathbf{x}_{\text{chirp}}. \tag{18}$$

C. Chirp Domain Problem

From (17), it is seen that each data carrier in the chirp domain is shifted by an amount of $l + k$. However, this property poses a significant problem for channel estimation, particularly when considering the resolvability of the channel taps, fractional delay, and Doppler shifts.

1) Resolvability of Channel Taps: This problem appears in the case of having two or more channel taps with the same sum of delay and Doppler (i.e., $(l_i + k_i = l_j + k_j; i \neq j)$). The scenario of superimposing an unknown number of channel taps creates an extremely complex issue in resolving channel taps. The overlapping of these taps at the receiver presents itself as a one-tap channel, making it impossible to obtain accurate channel estimation in the chirp domain. Any attempt to perform channel equalization under these conditions in the chirp domain leads to severe system performance degradation. It is critical to address this issue to ensure the system's optimal performance. Fig. 2 demonstrates two specific scenarios that arise from the phenomenon described. In Fig. 2(a), an OCDM signal is transmitted through a single-tap channel with l delay and $k = -l$ Doppler shift. The resulting signal is shifted by a time delay l (represented by the dashed pulse in the chirp domain) and then shifted back

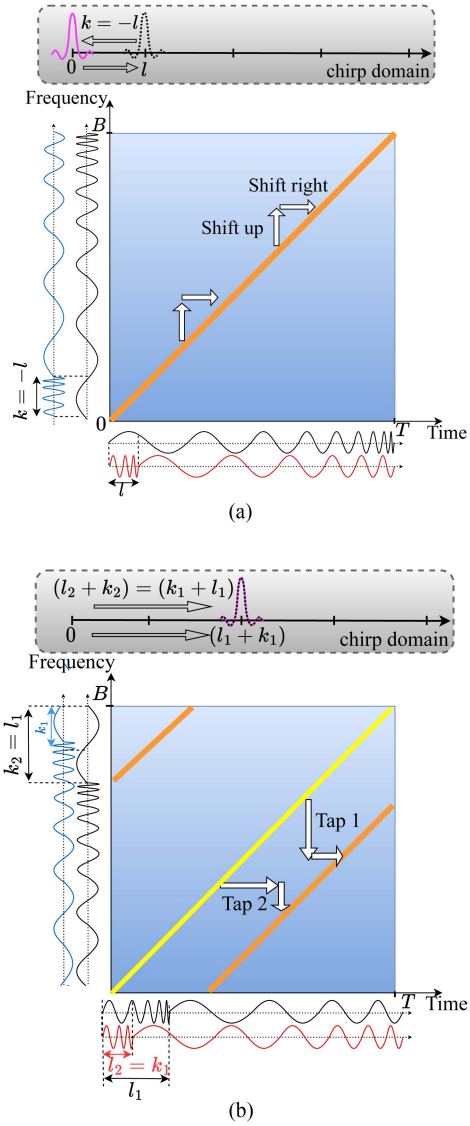

Fig. 2. Illustration of the problems associated with estimating the channel in chirp domain. (a) Resolvability of channel taps problem. (b) Selective-dispersive channel problem.

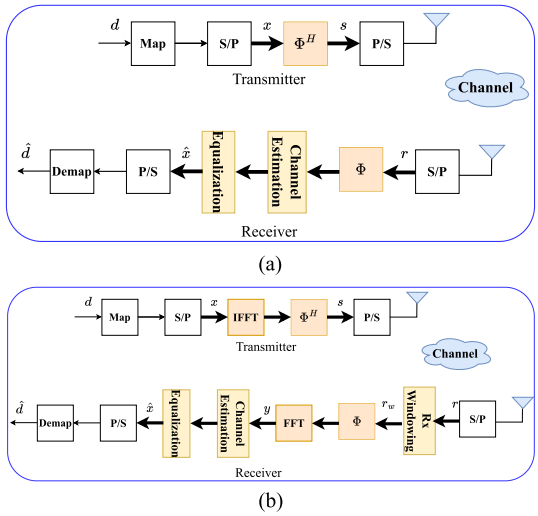

Fig. 3. Block diagram for the OCDM transceiver design. (a) Conventional. (b) Proposed.

by a negative Doppler shift (represented by the colored pulse in the chirp domain) creating selectivity in the chirp domain. This indicates that the straightforward channel estimation of the delays and Doppler shifts in chirp domain might not be always correct since the shift of each channel tap is the sum of the delay and Doppler shift at the same time.

2) Selective-Dispersive Channel: The channel in chirp domain exhibits both selectivity and dispersion simultaneously. For instance, consider a single OCDM carrier being transmitted through a two-tap channel each having (l_1, k_1) and $(l_2 = k_1, k_2 = l_1)$ delay and Doppler shift, respectively. The received signal is represented by the superposition of two chirps as seen in Fig. 2(b), which corresponds to two superimposed pulses (dashed and colored pulse) in the chirp domain. This causes selectivity in chirp domain where different chirps will see different channel gains. To summarize, the channel in chirp is selective and dispersive as follows

$$h_{\text{chirp}} = \begin{cases} \text{Selective}, & l_j = k_i, k_j = l_i \ (\forall i, j \in [0, L-1]) \\ \text{Dispersive}, & \text{Otherwise} \end{cases}. \tag{19}$$

Therefore, analyzing and estimating the channel in chirp domain in conventional OCDM systems is extremely difficult and might not be efficient at all.

3) Fractional Shifts: This problem arises due to the fact that the spreading in the chirp domain is due to both delays l and Doppler shifts k. This means that in order to get a non-fractional channel at the receiver side, we have to ensure that both delays and Doppler shifts are simultaneously integers, or $l + k \in \mathcal{Z}$, which is almost impossible. To generalize, estimation and equalization of a conventional OCDM in a chirp-domain can be efficient only under static channels where there is no Doppler spread or a single Doppler shift. However, transmitting an OCDM signal throughout a time-variant channel requires modifying the current OCDM system.

III. Proposed OCDM Framework

This section proposes a novel OCDM transceiver design and a proper channel estimation method.

A. Proposed OCDM Transceiver Design

To address the problem of the received OCDM signal being shifted by the sum of delays and Doppler shifts, it is necessary to separate the delays and Doppler effects in the received signal. This separation is required to resolve the channel taps at the receiver. Based on the conventional OCDM transceiver in Fig. 3(a), we propose a pre-coded OCDM waveform, as seen in Fig. 3(b). The mapped data are pre-coded with an inverse discrete Fourier transform (IDFT) block before applying the IDFnT at the transmitter and a DFT block at the receiver. The transmitted

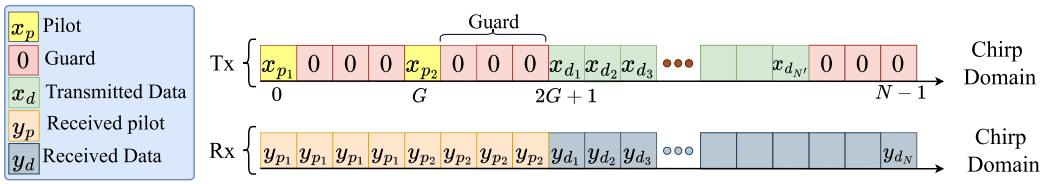

Fig. 4. Pilot and data symbols arrangements at the transmitter and receiver.

signal is redefined as follows

$$\mathbf{s} = \mathbf{\Phi}^H \mathbf{F}^H \mathbf{x}_{\text{chirp}}. \tag{20}$$

Passing the transmitted signal in a doubly-dispersive channel, and demodulating it gives a frequency domain signal given as

$$\mathbf{y} = \underbrace{\mathbf{F}\mathbf{\Phi}\mathbf{H}\mathbf{\Phi}^H\mathbf{F}^H}_{\mathbf{H}'_{\text{eff}}}\mathbf{x}_{\text{chirp}} + \mathbf{w}, \tag{21}$$

where the new domain effective channel $\mathbf{H}'_{\text{eff}}$ is given by

$$\begin{aligned} H'_{\text{eff}}(m,n) &= \sum_{l=0}^{N-1}\sum_{k=0}^{N-1}\sum_{i=0}^{L-1} F(m,l)H_{\text{eff}}F^H(k,n), \\ &= \sum_{i=0}^{L-1} h_i e^{-j\pi\frac{k_i^2}{N}} e^{-2j\pi\frac{n(l_i+k_i)+l_i k_i}{N}} \delta([m-n]_N - k_i). \end{aligned} \tag{22}$$

Based on (22), an input-output relationship is derived as shown below

$$\begin{aligned} y(m) &= \sum_{n=0}^{N-1} H'_{\text{eff}}(m,n)x(n), \\ &= \sum_{i=0}^{L-1} \hbar_i e^{-j\frac{2\pi}{N}m(l_i+k_i)} x\left([m-k_i]_N\right) + w(m). \end{aligned} \tag{23}$$

By comparing the received signal in (23) and in (16), it is seen that the shift in the chirp domain is k for the proposed waveform while it is equal to $k+l$ for the conventional OCDM. This makes the proposed OCDM system advantageous to the conventional one in two ways, as follows:

1) Having fractional delays in the channel will not cause interference or spread between the data in chirp domain.
2) The channel becomes easier to estimate from (23), as will be explained in the following subsection.

B. Proposed Embedded Pilot Channel Estimation

Inspired by the work in [19], in this paper, we propose an embedded double-impulse pilot channel estimation where two pilot symbols are used to estimate the channel and they are given by $x_{p_q}(m) = \sqrt{E_{p_q}}\delta(m - m_{p_q})$, $q = \{1, 2\}$ with signal-to-noise ratio (SNR): $\text{SNR}_p = E_{p_q}/\sigma^2$, where E_{p_q} and m_{p_q} denote the power and the location of the pilots. The two pilots are transmitted within the data frame, and a guard is added to eliminate the interference from the data after passing through the wireless channel and to prevent inter-symbol interference (ISI) between the two pilots, as shown in Fig. 4. The proposed OCDM frame along with the pilot, guard, and data symbols arrangements is given as

$$x(m) = \begin{cases} x_p, & m = m_{p_1},\, m = m_{p_2} \\ 0, & m \in [(m_{p_1}+G) \cup (m_{p_2}+G)], \\ x_d, & \text{otherwise} \end{cases} \tag{24}$$

where $G = k_{\max}$ is the guard interval.

At the receiver, the pilot signal is truncated from the chirp-domain received signal and it is given by

$$\begin{aligned} y_p(m) = \sum_{q=1}^{2}\sum_{i=0}^{L-1} &\sqrt{E_{p_q}}\hbar_i e^{-j\frac{2\pi}{N}k_i(l_i+k_i)} e^{-j\frac{2\pi}{N}\left(m_{p_q}-1\right)(l_i+k_i)} \\ &\times \delta\left([m - m_{p_q} - k_i]_N\right) + w(m). \end{aligned} \tag{25}$$

Since the guard G is designed to eliminate the ISI, the received signal from (25) can be separated into two signals corresponding to the output due to each pilot. These q-th signal corresponding to the q-th pilot is found as

$$\begin{aligned} v_{p_1}(m') = \sum_{i=0}^{L-1} &\sqrt{E_{p_1}}\hbar_i e^{-j\frac{2\pi}{N}k_i(l_i+k_i)} e^{-j\frac{2\pi}{N}\left(m_{p_1}-1\right)(l_i+k_i)} \\ &\times \delta\left([m - m_{p_1} - k_i]_N\right) + w(m), \end{aligned} \tag{26}$$

$$\begin{aligned} v_{p_2}(n') = \sum_{i=0}^{L-1} &\sqrt{E_{p_2}}\hbar_i e^{-j\frac{2\pi}{N}k_i(l_i+k_i)} e^{-j\frac{2\pi}{N}\left(m_{p_2}-1\right)(l_i+k_i)} \\ &\times \delta\left([m - m_{p_2} - k_i]_N\right) + w(m), \end{aligned} \tag{27}$$

where $m' = m - m_{p_1} \in [0, G]$ and $n' = m - m_{p_2} \in [0, G]$.

In addition, a threshold-based technique is used to combat the effect of the noise as follows

$$v_{p_q}(n) = \begin{cases} v_{p_q}(n_i), & |v_{p_q}(n)| > \zeta \\ 0, & \text{otherwise} \end{cases}, \tag{28}$$

where ζ is the threshold; the selection of the threshold is going to be emphasized later in simulation section. The estimated channel parameters are obtained as follows

1) Estimating Doppler Shifts: The Doppler shifts are estimated using only one pilot. Since the received impulse pilot signal is shifted by delays equal to k_i, the Doppler shifts k_i are the indices of the non-zero elements of the received pilot p_1 after applying the threshold.

2) Estimating Delay Shifts: The delays are estimated by applying an element-wise division between v_{p_1} and v_{p_2}, we find

$$\hat{l}_i + \hat{k}_i = \frac{N \ln\left(\frac{v_{p_2}(n_i)}{v_{p_1}(n_i)}\right)}{j2\pi(m_{p_2} - m_{p_1})}. \tag{29}$$

Algorithm 1: The Proposed Channel Estimation Framework.

Input: $\mathbf{Y}$
Output: l_i, k_i, and h_i.
Extract $\mathbf{Y}_p$ from $\mathbf{Y}$ as in (25).
Truncate the received signal for each pilot as in (26) and (27).:
  for $m - m_{p_1} = 0, 1, \ldots, G$ **do**
    Compute v_{p_1} as in (26)
  for $m - m_{p_2} = 0, 1, \ldots, G$ **do**
    Compute v_{p_2} as in (27)
Apply threshold to the received pilots signals as in (28):
  for $n = 0, 1, \ldots, G$ **do**
    Compute v_{p_q} as in (28)
Estimate Channel parameters:
  for $0 = 0, 1, \ldots, L-1$ **do**
    Compute k_i as in III-B1
    Compute l_i as in (29)
    Compute h_i as in (30)

Since the Doppler shifts k_i are estimated in the previous step, estimating the delays l_i from (29) becomes trivial.

3) Estimating Channel Coefficients: The channel coefficients are found straightforward as follows

$$\hat{h}_i = \frac{v_{p_1}(n_i)}{\sqrt{E_p}\Gamma}, \tag{30}$$

where $\Gamma = e^{-j\frac{\pi k_i^2}{N}} e^{-j\frac{2\pi}{N}k_i l_i}$. The channel estimation framework is summarized in Algorithm 1.

C. Channel Equalization

The channel equalization process can be done using one of the following techniques:

1) MMSE Detection: Conventional MMSE detector can be used to equalize the channel effects using the estimated effective channel $\hat{\mathbf{H}}_{\text{eff}}$. The estimated data symbols are obtained by [20]

$$\hat{\mathbf{x}} = \hat{\mathbf{H}}_{\text{eff}}^H \left(\hat{\mathbf{H}}_{\text{eff}} \hat{\mathbf{H}}_{\text{eff}}^H + \sigma^2 \boldsymbol{I}_N \right)^{-1} \mathbf{y}. \tag{31}$$

2) MP Detection Algorithm: Based on the vectorized form of the received signal in (10), we propose a MP algorithm for the OCDM signal using the input-output relation in (16). Due to the sparse nature of the OCDM chirp-domain effective channel, where only L elements out of N are non-zero in each row and column of the sparse matrix $\mathbf{H}_{\text{eff}}$. The detection method of the joint maximum a posterior probability (MAP) for estimating the transmitted data is given by

$$\hat{x} = \underset{x \in \mathcal{A}^{N\times 1}}{\text{argmax}} Pr(\mathbf{x}|\mathbf{y}, \mathbf{H}_{\text{eff}}), \tag{32}$$

where $\mathcal{A}$ is the set of constellation symbols. Using Bayes theorem and assuming all the symbols are equiprobable, (32) can be rewritten as

$$\hat{x} \approx \underset{x \in A^{N\times 1}}{\text{argmax}} \prod_{m \in \mathcal{J}_n} Pr(y(m)|x(n) = a_j, \mathbf{H}_{\text{eff}}). \tag{33}$$

In order to find a solution for the approximate MAP estimation in (33), we follow the MP algorithm in [21], by modeling the OCDM system as a connected factor graph node with N check nodes representing the received signal $\mathbf{y}$, and N variable nodes representing transmitted signal $\mathbf{x}$ [21].

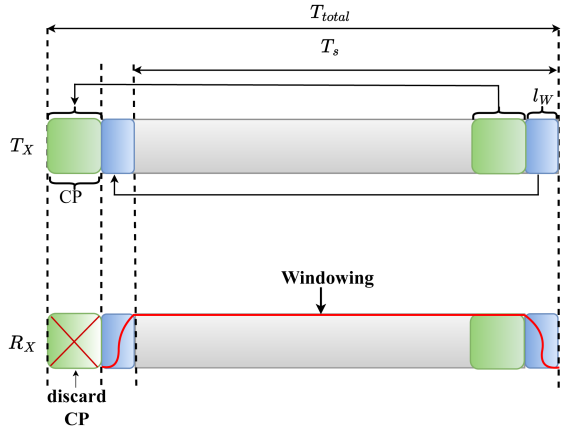

Fig. 5. Normalized mean square error (NMSE) comparison under doubly-dispersive channel with different channel taps.

IV. Proposed Windowed-OCDM for Fractional Doubly-Dispersive Channels

In practical wireless communication, transmitting a signal through a doubly dispersive channel causes the signal to experience both fractional delays and fractional Doppler shifts, in which case using a conventional OCDM receiver can significantly degrade the system's performance. To address the problem of mitigating these effects, a wideband system can be used to provide a sufficient delay resolution, therefore ensuring only integer delay shifts occur after sampling the received signal. On the other hand, mitigating the effects of fractional Doppler shifts is not straightforward. To compensate for the effect induced by fractional Doppler shifts on the received signal, we propose a time-domain windowing mechanism to surpass the effect of side lobe tails and approximate the effect of fractional Doppler to an integer Doppler effect.

The vectorial form of the pulse shaped OCDM time domian signal s is given as

$$\mathbf{s} = \mathbf{\Phi}^H \mathbf{F}^H \mathbf{x}_{\text{chirp}}. \tag{34}$$

Later a guard is appended to the beginning of the the frame as shown in Fig. 5. Let $G = CP + l_w$ be the utilized guard where CP corresponds to cyclic prefix to combat the effect of ISI which is greater than the maximum excess delay of the channel $l_{\max}$, and l_w defines the transition state of the applied window. To get the OCDM time domain after guard insertion $\mathbf{s}_f$ a matrix manipulation is applied as follows

$$\mathbf{s}_f = \mathbf{M}\mathbf{s} = \mathbf{M}\mathbf{\Phi}^H \mathbf{F}^H \mathbf{x}_{\text{chirp}}. \tag{35}$$

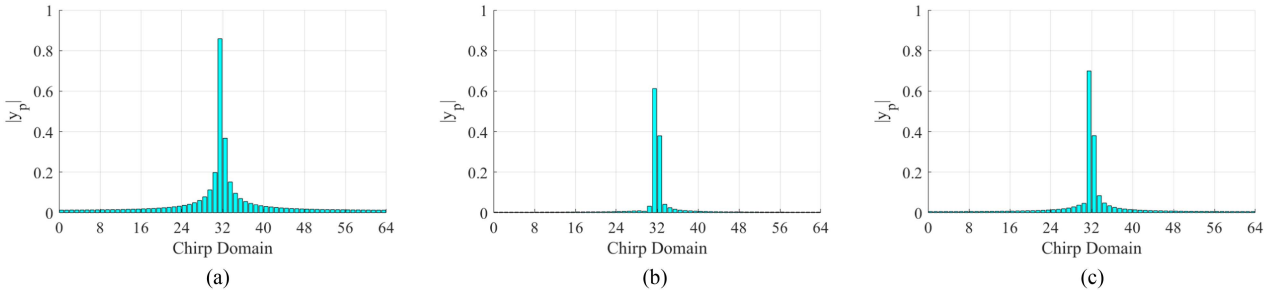

Fig. 6. OCDM pulse chirp domain response using different windows under 1 tap channel with fractional Doppler. (a) No window. (b) Kaiser window. (c) RC window.

where M is the guard addition matrix defined as

$$\mathbf{M} = \begin{bmatrix} \mathbf{0}_{G\times(N-G)} & \mathbf{I}_G \\ & \mathbf{I}_N \end{bmatrix}. \tag{36}$$

At the receiver, firstly the CP is discarded from the received signal by applying a matrix removal technique as given below

$$\mathbf{r}_{CP} = \mathbf{Dr} = \mathbf{DHS_f}, \tag{37}$$

where D is the CP removal matrix defined as

$$\mathbf{D} = \begin{bmatrix} \mathbf{0}_{(N)\times(G)} & \mathbf{I}_N \end{bmatrix}. \tag{38}$$

Then a windowing process is applied as indicated with the red line as illustrated in Fig. 5. The windowing process is established with point by point multiplication of the diagonal windowing matrix $\mathbf{W} \in \mathcal{C}^{(N+l_m)\times(N+L_m)}$ with the vectorized received signal. The received signal after windowing is given by

$$\mathbf{r}_w = \mathbf{Wr} = \mathbf{WHS} = \mathbf{M\Phi}^H\mathbf{F}^H\mathbf{x}_{\text{chirp}}. \tag{39}$$

The $\mathbf{W}$ non-zero entries are defined based on the deployed matrix. For the sake of comparison two windowing techniques are defined as follows

$$w_{RC}[k] = \begin{cases} \frac{1}{2}\left(1+\cos\left(\pi+\frac{k\pi}{l_w}\right)\right), & k=-l_w,\ldots,-1 \\ 1, & k=0,\ldots,N-l_W+1 \\ \frac{1}{2}\left(1+\cos\left(\pi+\frac{k\pi}{l_w}\right)\right), & k=N-l_w,\ldots N-1 \end{cases} \tag{40}$$

$$w_{KW}[k] = \frac{J_0(0)\left(\beta\sqrt{1-\left(\frac{k-\frac{N}{2}}{\frac{N}{2}}\right)^2}\right)}{J_0(\beta)}, \quad k=-l_m,\ldots,0,1,\ldots,N-1 \tag{41}$$

where, $w_{RC}[k]$ and $w_{KW}[k]$ represents the diagonal elements of the Raised Cosine (RC) window and kaiser-Bessel window, respectively. The choose of windows is based on the fact that RC window is presented on the only work that addressed the effect of windowing to mitigate fractional Doppler effect in OTFS waveform [22]. For the kaiser-Bessel window is implemented as it is proven to have a high side lobe interference suppression and a well localized OFDM transmission while approaching the interference-free BER performance [23], [24]. As windowing in time affects the localization in Delay Doppler domain where it suppress the effect of fractional Doppler [22], and since both OTFS and OCDM are both a precoded OFDM a localization of the OCDM pulse in chirp domain under fractional Doppler is feasible to occur using windowing, which is illustrated in Fig. 6 where applying Kaiser window in time domain suppresses the spread induced by fractional Doppler in chirp domain, even for multi tap channel the Kaiser window can provide a good localization in chirp domain as shown in Fig. 7. On the other side, RC window can suppress the spreading but at a very low rate making the spread sill affecting the whole frame. Based on the obtained results and analysis the Kaiser is most suitable when it comes to suppression of the spread effect, although it is at the expense of bandwidth excess as shown in Fig. 8 but the gain in this case is much more valuable.

V. Analysis and Simulation Results

In this section, we investigate the performance of the proposed channel estimation technique in OCDM system under doubly dispersive channel with fractional Doppler. The system is evaluated in terms of computational complexity, the NMSE of the estimated channel, and BER performances. binary phase shift keying (BPSK) modulation is considered in the simulations with a frame size of $N = 1024$.

A. Computational Complexity

The complexity overhead is evaluated in terms of computational complexity and time complexity for both channel estimation and channel equalization steps:

1) Channel Estimation: First, truncating the pilot signal from the received signal and obtaining the signal corresponding to each pilot has a complexity order of $\mathcal{O}(2(G+1))$. In the next step, the computational complexity of applying a threshold filter to each pilot signal is $\mathcal{O}(2(G+1))$. The element-wise division of the non-zero elements of each vector (after applying the threshold) is considered to have a complexity of $\mathcal{O}(L)$. Then, after extracting the delays and channel coefficients, which all have a total complexity of $\mathcal{O}(2L)$, the Doppler shifts are computed with the application of threshold. The general channel estimation framework has a total computational complexity of $\mathcal{O}(4(G+1)+3L)$. For time complexity it is proportional to

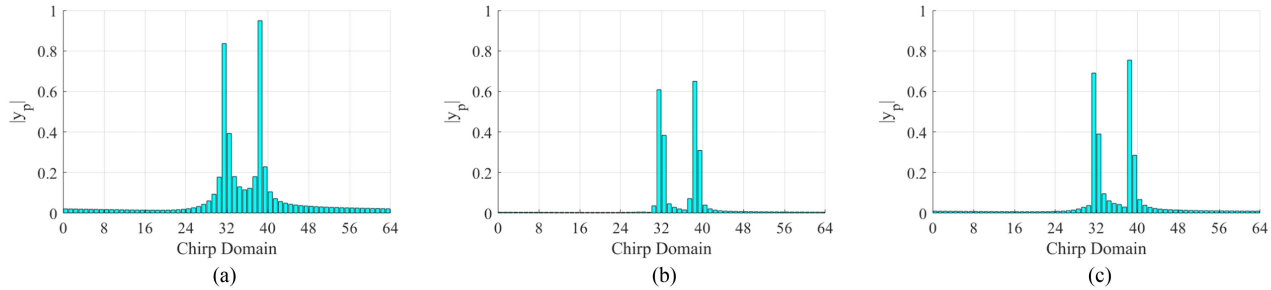

Fig. 7. OCDM pulse chirp domain response using different windows under 2 tap channel with fractional Doppler. (a) No windowing. (b) Kaiser window. (c) RC window.

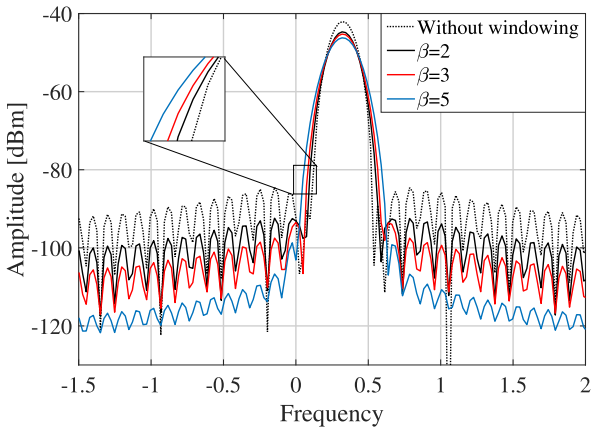

Fig. 8. Power spectrum of 1 OCDM carrier under different tuning parameter β.

computational complexity, since the the algorithm doesn't have any nested loops its time complexity is expected to $\mathcal{O}(2G+L)$ units of time.

2) Channel Equalization: The complexity overhead of the proposed framework is evaluated in two steps. Calculating the inverse of the $\hat{\mathbf{H}}_{\text{eff}}$ matrix in the MMSE detector requires a computational complexity of order $\mathcal{O}(N^3)$, which is not feasible for large frame size N. MP detector is used, which is shown to have a lower computational complexity in sparse channels [21]. The computational complexity of MP detector is calculated based on the algorithm steps as mentioned in [25]. First, the variance and probability mass function (PMF) each have a complexity order of $\mathcal{O}(NLQ)$, where Q is the modulation constellation cardinally. While computing the convergence indicator and updating the decision of the transmitted signal, each has a complexity of the order $\mathcal{O}(NQ)$, which gives a total MP algorithm complexity order $\mathcal{O}(n_{iter}NLQ)$.

Table I summarizes the computational complexities of channel estimation and equalization.

TABLE I
THE COMPUTATIONAL COMPLEXITIES OF CHANNEL ESTIMATION AND EQUALIZATION

		Computational Complexity
Channel estimation		$\mathcal{O}(4(G+1)+3L)$
Channel equalization	MMSE	$\mathcal{O}(N^3)$
	MAP	$\mathcal{O}(n_{iter}NLQ)$

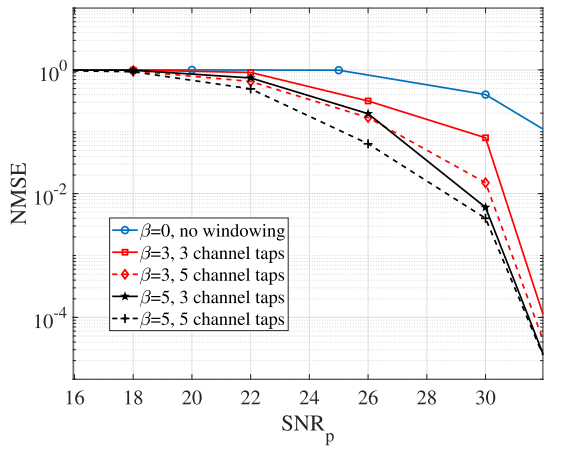

Fig. 9. NMSE comparison under different channel taps.

B. Channel NMSE Performance

In order to evaluate the performance of the proposed channel estimation framework in a doubly dispersive channel with random separation between channel taps and fractional Doppler, the assessment of the NMSE of the estimated channel both with and without the use of a windowing block is done. the NMSE is also analyzed for different channel tap numbers and window tuning parameters, as shown in Fig. 9. The obtained results demonstrate a significant improvement in minimizing the estimation error as SNR increases, where for an optimal SNR range of $[26-32]$dB, good estimation of the channel is found. It is worth noting that without the use of the windowing block, the performance of the channel estimation technique degrades due to the side lobes induced by fractional Doppler, which made it difficult to distinguish the channel taps. Furthermore, Fig. 9 indicates that OCDM can exploit the diversity gain of the channel, as the number of multipath increases, lower values of NMSE are obtained.

C. BER Performance

In Fig. 10 a BER comparison between conventional OCDM in [10] and the proposed OCDM with and without channel

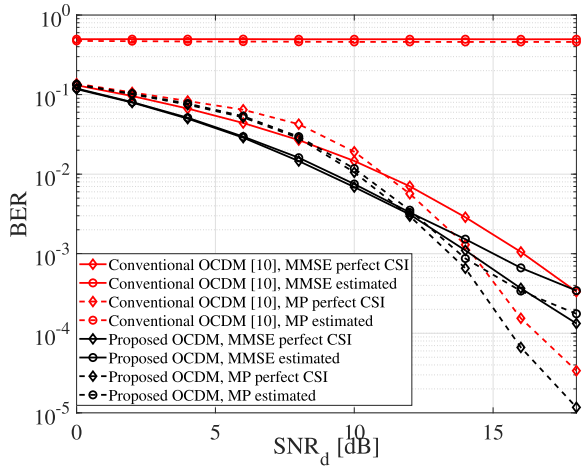

Fig. 10. BER versus SNR$_d$ analysis.

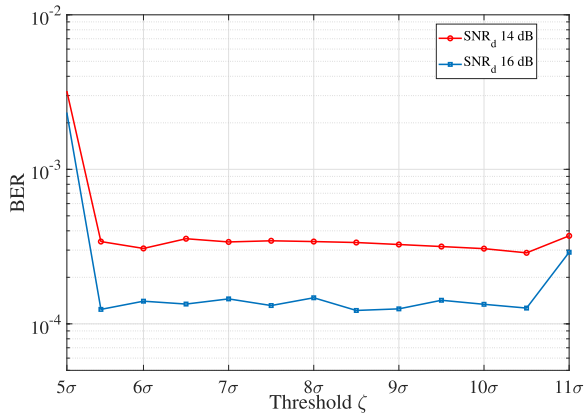

Fig. 11. BER versus channel estimation threshold analysis.

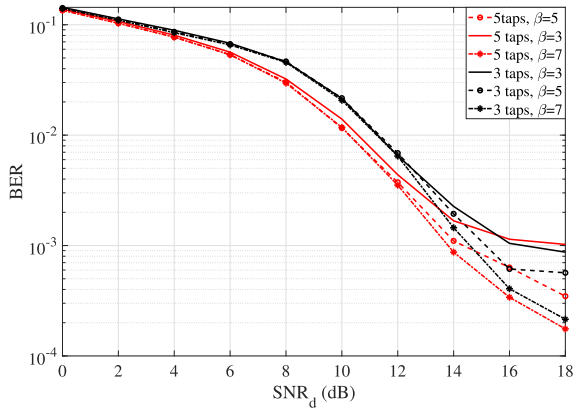

Fig. 12. BER vs SNR$_d$ analysis for different values of β.

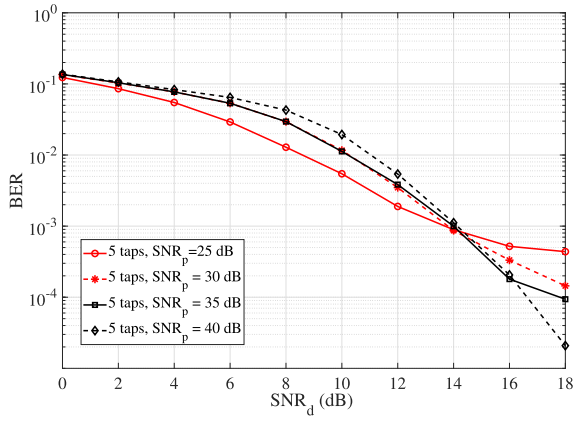

Fig. 13. BER vs SNR$_d$ analysis for different SNR$_p$ ($L = 5$).

information to test the communication reliability of the two systems. It is shown that in the absence of channel information the conventional OCDM suffers from a huge degradation in the BER performance under doubly dispersive channel, which proves what is concluded in Section II that in a random channel OCDM suffers from the inseparability of channel taps. On the other hand, the proposed OCDM system gives optimum performance in the absence of channel information near to the perfect channel state information (CSI) even under a doubly dispersive channel with a random separation between channel taps and the presence of fractional Doppler.

Fig. 10 also shows the superiority of using MP equalizer compared to the conventional MMSE equalizer, where MP leverages a better performance in perfect CSI or without channel information compared to MMSE.

Next, the effect of the threshold ζ on the performance of the channel estimation framework is investigated as seen in Fig. 11. The threshold varies as a function of the noise variance σ to establish a more meaningful relationship between the threshold filter and the signal noise. For small values of ζ the BER degrades as the noise interferes with the detection of the data. As ζ increases, BER performance improves, but until a certain level of ζ where the performance of BER degrades again, this occurs because increasing the threshold prevents the detection of low power channel paths.

The impact of different window tuning parameters β on system performance is illustrated in Fig. 12. As shown, increasing β results in an improvement in the BER performance of the MP equalizer. This improvement is directly related to the accuracy of the channel estimation, which is enhanced by better pilot pulse localization achieved through a high value of β. In other words, when β is high, the localization of the received pilot signal becomes more precise, leading to more accurate channel estimation and consequently, better performance of the MP equalizer in terms of BER. Overall, the results in Fig. 12 indicate that the selection of an appropriate value for β is crucial in enhancing the system performance.

Next, the impact of the proper pilot SNR value on the performance of the MP equalizer is investigated as shown in Fig. 13. The value of SNR$_p$ has a significant effect on the BER performance of the equalizer. This effect can be attributed to the channel estimation framework, which relies on threshold filtering, making it more accurate in the presence of less noise. However, it is not practical to increase the value of SNR$_p$ indefinitely. Instead, it is more reasonable to choose a value between 30 dB and 35 dB, which yields reasonable results while remaining feasible.

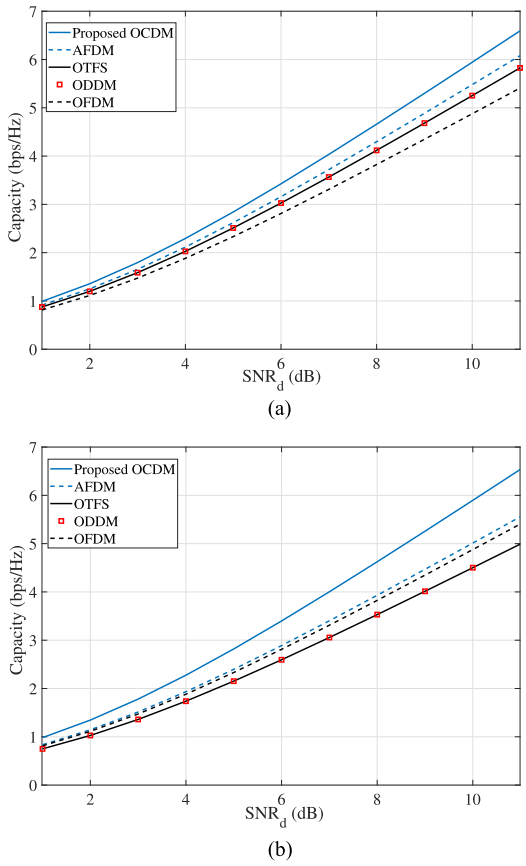

Fig. 14. Capacity performance for proposed OCDM, AFDM, and [17] with (a) $k_{\max} = \sqrt{N}/8$, (b) $k_{\max} = \sqrt{N}/4$.

D. Spectral Efficiency

The spectral efficiency (SE) of a waveform is influenced by several factors, including the frame length, cyclic prefix (CP) size, and pilot guard length. Based on the formula of SE given in [26], the SE of OCDM is calculated for a given signal-to-noise ratio (SNR) Γ, as follows

$$SE_{OCDM} = \left(\frac{N-(\alpha)}{N}\right)\log_2(1+\Gamma), \tag{42}$$

where α represents the length of the channel estimation overhead. For the proposed work in this paper, α is equal to $2k_{\max}+2$ as depicted in Fig. 4. The SE of AFDM is calculated using their proposed overhead [9], where in AFDM an $\alpha = 2(l_{\max}+1)(2(k_{\max}+\zeta_v)+1)-1$; with $\zeta_v = 8$ provides the best performance, is proposed. In addition and for the sake of comparison we adopted the the reduced CP SE formulas as in [26] for both OTFS and ODDM as they are both a delay-Doppler (DD) domain based waveforms.

Fig. 14(a) depicts a significant advantage over the other compared waveforms due to the reduced overhead for channel estimation, even in the presence of large Doppler spread as in Fig. 14(b), the proposed OCDM suffers only from a slight degradation in SE compared to the other waveforms.

VI. Conclusion

This article investigates the input-output relationship of the OCDM waveform and demonstrates that the circular convolution property of the Fresnel transform can be generalized for doubly dispersive channels. The work further demonstrates the joint selectivity and dispersiveness of the effective channel in the chirp domain and elaborates on the difficulties of channel estimation and equalization of OCDM in the presence of fractional Doppler spread. According to this, a novel OCDM system based on additional FFT and windowing blocks is proposed that ensures effective channel sparsity. Then, a spectrally efficient channel estimation scheme is designed based on embedded pilots that allow the proposed OCDM system to perform efficiently under doubly dispersive channels. As a future direction, the chirp properties of radar could be leveraged to enhance the OCDM waveform for joint sensing and communication (JSAC) applications.

References

[1] J. Thompson et al., "5G wireless communication systems: Prospects and challenges [Guest Editorial]," *IEEE Commun. Mag.*, vol. 52, no. 2, pp. 62–64, Feb. 2014.
[2] D. Gan, X. Ge, and Q. Li, "An optimal transport-based federated reinforcement learning approach for resource allocation in cloud-edge collaborative IoT," *IEEE Internet Things J.*, vol. 11, no. 2, pp. 2407–2419, Jan. 2024.
[3] Z. E. Ankarali, B. Peköz, and H. Arslan, "Flexible radio access beyond 5G: A. future projection on waveform, numerology, and frame design principles," *IEEE Access*, vol. 5, pp. 18295–18309, 2017.
[4] M. Chafii, L. Bariah, S. Muhaidat, and M. Debbah, "Twelve scientific challenges for 6G: Rethinking the foundations of communications theory," *IEEE Commun. Surveys Tuts.*, vol. 25, no. 2, pp. 868–904, Secondquarter 2023.
[5] R. Bomfin, M. Chafii, A. Nimr, and G. Fettweis, "A robust baseband transceiver design for doubly-dispersive channels," *IEEE Trans. Wireless Commun.*, vol. 20, no. 8, pp. 4781–4796, Aug. 2021.
[6] R. Hadani and A. Monk, "OTFS: A. new generation of modulation addressing the challenges of 5G," 2018, *arXiv:1802.02623*.
[7] K. R. Murali and A. Chockalingam, "On OTFS modulation for high-Doppler fading channels," in *Proc. IEEE Inf. Theory Appl. Workshop*, 2018, pp. 1–10.
[8] H. Lin and J. Yuan, "Orthogonal delay-doppler division multiplexing modulation," *IEEE Trans. Wireless Commun.*, vol. 21, no. 12, pp. 11024–11037, Dec. 2022.
[9] A. Bemani, N. Ksairi, and M. Kountouris, "Affine frequency division multiplexing for next generation wireless communications," *IEEE Trans. Wireless Commun.*, vol. 22, no. 11, pp. 8214–8229, Nov. 2023.
[10] X. Ouyang and J. Zhao, "Orthogonal chirp division multiplexing," *IEEE Trans. Commun.*, vol. 64, no. 9, pp. 3946–3957, Sep. 2016.
[11] M. S. Omar and X. Ma, "Performance analysis of OCDM for wireless communications," *IEEE Trans. Wireless Commun.*, vol. 20, no. 7, pp. 4032–4043, Jul. 2021.
[12] M. S. Omar and X. Ma, "Spectrum design for orthogonal chirp division multiplexing transmissions," *IEEE Wireless Commun. Lett.*, vol. 9, no. 11, pp. 1990–1994, Nov. 2020.
[13] X. Wang, X. Shen, F. Hua, and Z. Jiang, "On low-complexity MMSE channel estimation for OCDM systems," *IEEE Wireless Commun. Lett.*, vol. 10, no. 8, pp. 1697–1701, Aug. 2021.
[14] M. S. Omar and X. Ma, "Pilot symbol aided channel estimation for OCDM transmissions," *IEEE Commun. Lett.*, vol. 26, no. 1, pp. 163–166, Jan. 2021.
[15] R. Zhang, Y. Wang, and X. Ma, "Channel estimation for OCDM transmissions with carrier frequency offset," *IEEE Wireless Commun. Lett.*, vol. 11, no. 3, pp. 483–487, Mar. 2022.
[16] B. Wang and X. Guan, "Channel estimation for underwater acoustic communications based on orthogonal chirp division multiplexing," *IEEE Signal Process. Lett.*, vol. 28, pp. 1883–1887, 2021.

[17] L. Giroto de Oliveira et al., "Discrete-fresnel domain channel estimation in OCDM-based radar systems," *IEEE Trans. Microw. Theory Techn.*, vol. 71, no. 5, pp. 2258–2275, May 2023.
[18] S. Bhattacharjee, K. V. Mishra, R. Annavajjala, and C. R. Murthy, "Multi-carrier wideband OCDM-based THz automotive radar," in *Proc. IEEE Int. Conf. Acoust., Speech, Signal Process.*, 2023, pp. 1–5.
[19] P. Raviteja, K. T. Phan, and Y. Hong, "Embedded pilot-aided channel estimation for OTFS in delay–Doppler channels," *IEEE Trans. Veh. Technol.*, vol. 68, no. 5, pp. 4906–4917, May 2019.
[20] L. Rugini, P. Banelli, and G. Leus, "Simple equalization of time-varying channels for OFDM," *IEEE Commun. Lett.*, vol. 9, no. 7, pp. 619–621, Jul. 2005.
[21] P. Raviteja, K. T. Phan, Y. Hong, and E. Viterbo, "Interference cancellation and iterative detection for orthogonal time frequency space modulation," *IEEE Trans. Wireless Commun.*, vol. 17, no. 10, pp. 6501–6515, Oct. 2018.
[22] A. Tusha and H. Arslan, "Low complex inter-doppler interference mitigation for OTFS systems via global receiver windowing," *IEEE Trans. Veh. Technol.*, vol. 72, no. 6, pp. 7685–7698, Jun. 2023.
[23] R. S. Yarrabothu and U. R. Nelakuditi, "Optimization of out-of-band emission using kaiser-bessel filter for UFMC in 5G cellular communications," *China Commun.*, vol. 16, no. 8, pp. 15–23, 2019.
[24] E. Güvenkaya, E. Bala, R. Yang, and H. Arslan, "Time-asymmetric and subcarrier-specific pulse shaping in OFDM-based waveforms," *IEEE Trans. Veh. Technol.*, vol. 64, no. 11, pp. 5070–5082, Nov. 2014.
[25] S. S. Das and R. Prasad, *Orthogonal Time Frequency Space Modulation: OTFS a Waveform for 6G*. Boca Raton, FL, USA: CRC Press, 2022.
[26] S. E. Zegrar and H. Arslan, "A novel cyclic prefix configuration for enhanced reliability and spectral efficiency in OTFS systems," *IEEE Wireless Commun. Lett.*, vol. 12, no. 5, pp. 888–892, May 2023.